NHS Breast Screening Programme

NHS
Cancer Screening Programmes

Technical evaluation of Hologic Selenia Dimensions 2-D digital breast imaging system

NHSBSP EQUIPMENT REPORT 1101

FEBRUARY 2011

TECHNICAL EVALUATION OF HOLOGIC SELENIA DIMENSIONS 2-D DIGITAL BREAST IMAGING SYSTEM

NHSBSP Equipment Report 1101
February 2011

Authors
K C Young, J M Oduko, L Warren
all of the National Coordinating Centre for the Physics of Mammography, Guilford

Enquiries
Enquiries about this report should be addressed to:

Professor KC Young
National Coordinating Centre for the Physics of Mammography
Medical Physics Department
Royal Surrey County Hospital
Guildford
GU2 7XX

Tel: 01483 408310
Fax: 01483 406742
Email: ken.young@nhs.net
Website: www.nccpm.org

Published by
NHS Cancer Screening Programmes
Fulwood House
Old Fulwood Road
Sheffield
S10 3TH

Tel: 0114 271 1060
Fax: 0114 271 1089
Email: info@cancerscreening.nhs.uk
Website: www.cancerscreening.nhs.uk

ACKNOWLEDGEMENTS

The authors are grateful to the staff at the Hologic factory in Bedford, Massachusetts for their help in evaluating the equipment at their site.

CONTENTS

1. INTRODUCTION

1.1 Testing procedures and performance standards for digital mammography

This report is one of a series evaluating commercially-available digital mammography systems on behalf of the NHS Breast Screening Programme (NHSBSP). The testing methods and standards applied are derived chiefly from NHSBSP Equipment Report 0604.[1] The report is referred to in this document as the NHSBSP protocol and it uses the same image quality and dose standards as those provided in the European protocol.[2,3] The European protocol was followed where there is a more detailed performance standard: for example, for the automatic exposure control (AEC) system.

1.2 Objectives

The tests had two objectives: first to determine whether the Hologic Selenia Dimensions breast imaging system (hereafter Hologic Dimensions), operating in its two-dimensional imaging mode, meets the main standards in the NHSBSP and European protocols; second, to provide performance data for comparison with other products. The tomography performance of the system was not evaluated. Clinical evaluations are published separately by the NHSBSP where systems meet the minimum standards in the NHSBSP protocol. A final decision on the suitability of systems for use in the NHSBSP depends on a review of both the technical and clinical evaluations.

2. METHODS

2.1 System tested

The tests were conducted at the Hologic headquarters in Bedford, Massachusetts, USA, on the system shown in Figure 1 and described in Table 1. The detector is manufactured by Hologic, Inc.

Figure 1 Photograph of Hologic Dimensions.

Table 1 System description

Manufacturer	Hologic, Inc
Model	Dimensions
System serial number	81310080042
X-ray tube	Varian 113T
Target material	Tungsten
Added filtration	35 µm Rhodium 35 µm Silver
Detector type	Amorphous selenium
Detector serial number	W12810-77/MM60124
Pixel size	70 µm (in detector plane)
Detector area	Small: 166 x 216 mm Large: 216 x 266 mm
Pixel array	Small: 2560 x 3328 Large: 3328 x 4096
Pixel value offset	50
Source to detector distance	700 mm
Source to table distance	675 mm
AEC modes	Autofilter, Autotime*
AEC pre-exposure pulse	5mAs for CBT<5cm; 10mAs for CBT>=5cm
Software version	AWS:1.0.5.98\M35:1.0.8.19\GIP2D:3.8.0-4.8.3\GIP3D:1.0.3.2\SNRCNR:1.0.0.0-1.0.1.0\PMC:1.0.5.26\DET:1.0.10.2\DTC:1.0.0.9 \GCB:1.0.5.21\GEN:1.0.5.5\VTA:1.0.5.11\CRM:1.0.5.5 \T H:1.0.5.6\CDI:1.0.5.8\AIO:1.0.5.3\BKY:1.0.5.7

*Function of AEC modes: Autofilter selects kV and filter based on the compressed breast thickness. In Autotime mode, the kV and filter are chosen by the user. In both cases the pre-exposure pulse contributes to the dose to the patient but does not contribute to the formation of the image.

2.2 Output and half-value-layer (HVL)

The output and HVL were measured as described in the NHSBSP protocol, at intervals of 3kV for each target/filter combination.

2.3 Detector response

The detector response was measured as described in the NHSBSP protocol, with a 45 mm thickness of Perspex (polymethylmethacrylate or PMMA) placed at the tube exit port. An ion chamber was positioned above the table to determine the incident air kerma at the detector surface for a range of manually set mAs values at 28 kV, and for both target/filter combinations available (W/Rh and W/Ag). The readings were corrected to the surface of the detector using the inverse square law. No correction was made for attenuation by the table and detector cover. Images were saved as unprocessed files and transferred to another computer for analysis. A 10 mm square region of interest (ROI) was positioned on the mid-line and 6 cm from the chest wall edge of each image. The average pixel value and the standard deviation of pixel values within that region were measured. The relationship between average pixel values and the detector entrance surface air kerma was determined.

2.4 Dose measurement

Doses were measured using the X-ray set's automatic exposure control (AEC) to expose different thicknesses of PMMA. Each thickness had an area of 18 x 24 cm. The paddle height was adjusted to be equal to the equivalent breast thickness. Mean glandular doses (MGDs) were calculated for the equivalent breast thicknesses. To measure the contrast-to-noise ratio (CNR) an aluminium square, 10 mm x 10 mm and 0.2 mm thick, was placed on top of a 20 mm thick block, with one edge on the midline and 6 cm from the chest wall edge. Additional layers of PMMA were placed on top of these to vary the total thickness.

2.5 Contrast-to-noise ratio (CNR)

The images of the blocks of PMMA obtained during the dose measurement were analysed to obtain the CNRs. Twenty small square ROIs (approximately 2.5mm x 2.5mm) were used to determine the average signal and the standard deviations in the signal within the image of the aluminium square (4 ROI) and the surrounding background (16 ROI), as shown in Figure 2. Small ROIs are used to minimise distortions resulting from the heel effect and other causes of non-uniformity.[4] This is less important for DR systems than in computed radiography systems, however, because a flat-field correction is applied. The CNR was calculated for each image as defined in the NHSBSP and European protocols.

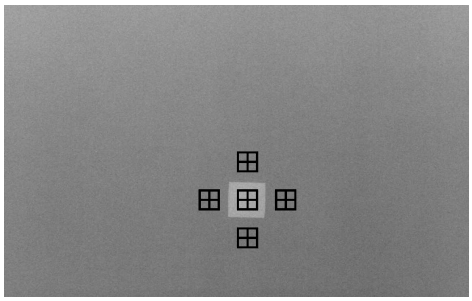

Figure 2 Location and size of ROI used to determine the CNR.

To apply the standards in the European protocol the limiting value for CNR (using 50 mm PMMA) was determined according to equation 1. This equation determines the CNR value ($CNR_{limiting\ value}$) that is necessary to achieve the minimum threshold gold thickness for the 0.1 mm detail (ie *threshold gold*$_{limiting\ value}$ = 1.68 µm which is equivalent to *threshold contrast*$_{limiting\ value}$ = 23.0% using 28 kV Mo/Mo). Threshold contrasts were calculated as described in the European protocol and used in equation 1.

$$CNR_{limiting\ value} = CNR_{measured} \times \frac{TC_{measured}}{TC_{limiting\ value}} \quad (1)$$

The relative CNR was then calculated according to equation 2 and compared with the limiting values provided for relative CNR shown in Table 2. The minimum CNR required to meet this criterion was then calculated.

$$Relative\ CNR = CNR_{measured}/CNR_{limiting\ value} \quad (2)$$

Table 2 Limiting values for relative CNR

Thickness of PMMA (mm)	Equivalent breast thickness (mm)	Limiting values for relative CNR (%) in European protocol
20	21	>115
30	32	>110
40	45	>105
45	53	>103
50	60	>100
60	75	>95
70	90	>90

2.6 AEC performance for local dense areas

The method used in the EUREF type testing protocol was followed. To simulate local dense areas nine images were made with different thicknesses (2–18 mm) of extra attenuation added, so that the compression plate remained in position at 40 mm height, as shown in Figure 3.

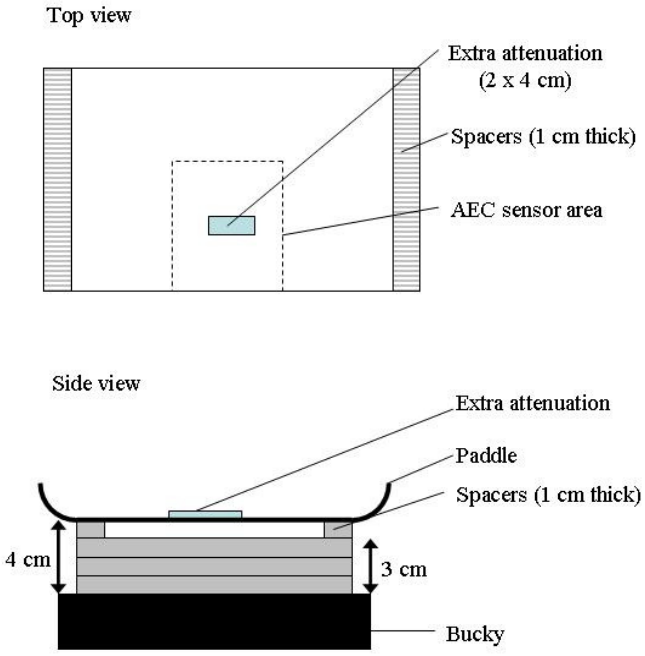

Figure 3 Set-up to measure AEC performance for local dense areas.

In the area of the extra attenuation (20 x 40 mm PMMA) the mean pixel value and standard deviation of a ROI of 2.5 x 2.5 mm were measured and the signal-to-noise ratio (SNR) calculated.

2.7 Noise analysis

The images acquired in the measurements of detector response using 28 kV W/Rh were used to analyse the image noise. Small ROI with an area of approximately 2.5 x 2.5mm were placed on the midline and 6cm from the chest wall edge. The average standard deviations of the pixel values in these ROI for each image were used to investigate the relationship between dose to the detector and image noise. It was assumed that this noise comprises three components – electronic noise, structural noise and quantum noise – with the relationship shown in equation 3. This method of analysis has been described previously.[5]

$$\sigma_p = \sqrt{k_e^2 + k_q{}^2 p + k_s{}^2 p^2} \quad (3)$$

where σ_p is the standard deviation in pixel values within an ROI with a uniform exposure and a mean pixel value p, and k_e, k_q and k_s are the coefficients determining the amount of electronic, quantum and structural noise in a pixel with a value p. For simplicity the noise is generally presented here as relative noise defined as in equation 4.

$$\textit{Relative noise} = \frac{\sigma_p}{p} \quad (4)$$

The variation in relative noise with mean pixel value was evaluated and fitted using equation 3, and non-linear regression used to determine the best fit for the constants and their asymptotic confidence limits (using GraphPad Prism Version 4.03 for Windows*). This established whether the experimental measurements of the noise fitted this equation, and the relative proportions of the different noise components. In fact, the relationship between noise and pixel values has been found empirically to be approximated by a simple power relationship as shown in equation 5.

$$\frac{\sigma_p}{p} = k_t p^{-n} \quad (5)$$

where k_t is a constant. If the noise were purely quantum noise the value of n would be 0.5. However the presence of electronic and structural noise means that n can be slightly higher or lower than 0.5.

The variance in pixel values within a ROI is defined as the standard deviation squared. The total variance was plotted against incident air kerma at the detector and fitted using equation 3. Again non-linear regression was used to determine the best fit for the constants and their asymptotic confidence limits, using the GraphPad Prism software.

* GraphPad Software, Inc, San Diego, California, USA, www.graphpad.com.

Using the calculated constants the structural, electronic and quantum components of the variance were estimated, assuming that each component was independently related to incident air kerma. The percentage of the total variance represented by each component was then calculated and plotted against incident air kerma at the detector. From this the dose range over which the quantum component dominates was estimated.

2.8 Image quality measurements

Contrast detail measurements were made using the CDMAM phantom.† The phantom was positioned with a 20 mm thickness of PMMA above and below, to give a total attenuation approximately equivalent to 50 mm of PMMA or 60 mm thickness of typical breast tissue. The kV target/filter combination and mAs were chosen to match as closely as possible that selected by the AEC when imaging a 5 cm thickness of PMMA. This procedure was repeated to obtain a representative sample of 16 images at this dose level. Unprocessed images were transferred to disk for subsequent analysis off-site. Further images of the test phantom were then obtained at other dose levels by manually selecting higher and lower mAs values with the same beam quality.

An automatic method of reading the CDMAM images was used.[5,6] The threshold gold thickness for a typical human observer was predicted using equation 6.

$$TC_{predicted} = r\ TC_{auto} \quad (6)$$

where $TC_{predicted}$ is the predicted threshold contrast for a typical observer and TC_{auto} is the threshold contrast measured using an automated procedure with CDMAM images. Contrasts were calculated from gold thickness for a nominal tube voltage of 28 kV and a Mo/Mo target/filter combination as described in the European protocol; r is the average ratio between human and automatic threshold contrast determined experimentally with the values shown in Table 3.[6]

Table 3 Values of *r* used to predict threshold contrast

Diameter of gold disc (mm)	Average ratio of human to automatically measured threshold contrast (*r*)
0.08	1.40
0.10	1.50
0.13	1.60
0.16	1.68
0.20	1.75
0.25	1.82
0.31	1.88
0.40	1.94
0.50	1.98
0.63	2.01
0.80	2.06
1.00	2.11

† Version 3.4, UMC St. Radboud, Nijmegen University, Netherlands

The main advantage of automatic reading is that it has the potential to eliminate observer error which is a significant problem when using human observers. However it should be noted that at the present time the official protocols are based on human reading.

The predicted threshold gold thickness for each detail diameter at each dose level was fitted with a curve as described in the NHSBSP protocol. The confidence limits for the predicted threshold gold thicknesses have been previously determined by a re-sampling method using a large set of images. The threshold contrasts quoted in the tables of results are derived from the fitted curves, as this has been found to improve accuracy.[6]

The expected relationship between threshold contrast and dose is shown in equation 7.

$$Threshold\ contrast = \lambda D^{-n} \quad (7)$$

D represents the MGD for a 60 mm thick standard breast equivalent to the test phantom configuration used for the image quality measurement, and λ is a constant to be fitted. It is assumed that a similar equation applies when using threshold gold thickness rather than contrast. This equation was plotted with the experimental data for each detail size from 0.1 to 1.0 mm. The value of *n* resulting in the best fit to the experimental data was determined.

The CDMAM images were also read by three experienced observers, who read four different images each for each dose level.

2.9 Image retention

Image retention was measured as described in the NHSBSP protocol. The regions used are shown in Figure 4.

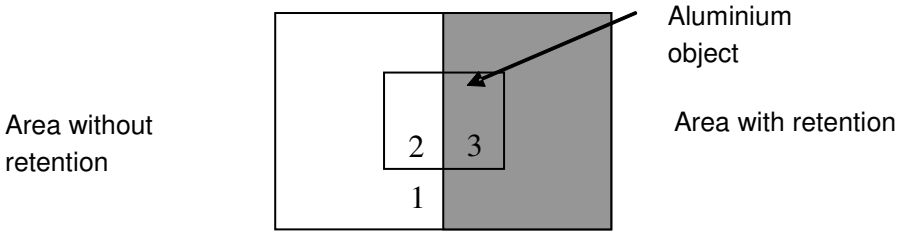

Figure 4 ROIs used for calculation of the image retention factor.

$$Image\ \ retention\ factor = \frac{mean\ pixel\ value\ (region\ 3) - mean\ pixel\ value\ (region\ 2)}{mean\ pixel\ value\ (region\ 1) - mean\ pixel\ value\ (region\ 2)} \quad (8)$$

2.10 Physical measurements of the detector performance

The modulation transfer function (MTF), normalised noise power spectrum (NNPS) and detective quantum efficiency (DQE) of the detector were measured. The methods used were as close as possible to those described by the International Electrotechnical Commission (IEC).[7] The radiation quality used for the measurements was adjusted by placing a uniform 2 mm thick aluminium filter at the tube housing. The beam quality used was 28 kV W/Rh. The test device to measure the MTF comprised a 0.8 mm thick

rectangle (120 mm x 60 mm) of stainless steel with polished straight edges. This test device was placed directly on the breast support table, and the grid was removed by selecting 'grid out' at the operator's console. The test device was positioned to measure the MTF in two directions, first perpendicular and then parallel to the chest wall edge. To measure the noise power spectrum the test device was removed and exposures made for a range of incident air kerma at the surface of the table. The DQE is presented as the average of the directions perpendicular and parallel to the chest wall.

2.11 Optimisation

A method for determining optimal beam qualities and exposure factors for digital mammography systems has been described previously and was used to evaluate this system.[4,5] CNR and mean glandular dose were measured as described above using blocks of PMMA from 20 to 70 mm thick. For each thickness four tube voltage settings were used (25, 28, 31 and 34 kV) with each of the target/filter combinations available and the mAs recorded. The MGDs to typical breasts with attenuation equivalent to each thickness of the PMMA were calculated as described in the NHSBSP protocol. Each exposure was designed to achieve a standard pixel value. The relationship between noise and pixel values in digital mammography systems has been previously[5] shown to be approximated by

$$\textit{Relative noise} = \frac{\sqrt{\frac{sd(bgd)^2 + sd(Al)^2}{2}}}{p} = k_t p^{-n} \qquad (9)$$

where k_t is a constant, and p is the average background pixel value linearised with absorbed dose to the detector. *sd(bgd)* is the average standard deviation of pixel values in the ROIs over the background. *sd(Al)* is the average standard deviation of pixel values in an ROI over a 0.2 mm x 10 mm x 10 mm piece of aluminium. The value of *n* was found by fitting this equation to the experimental data. Equation 10 was then used to calculate the dose required to achieve a target CNR, where *k* is a constant to be fitted, and *D* is the MGD for a breast of equivalent thickness.

$$CNR = kD^n \qquad (10)$$

The target CNR was that calculated to reach either the minimum or achievable image quality in the NHSBSP and European protocols using the following relationship.

$$\textit{Threshold contrast} = \frac{\lambda}{CNR} \qquad (11)$$

where λ is a constant that is independent of dose, beam quality and the thickness of attenuating material. The optimal beam quality for each thickness was selected as that necessary to achieve the target CNR for the minimum dose.

3. RESULTS

3.1 Output and HVL

The results are shown in Table 4.

Table 4 Output and HVL

kV T/F	Output (mGy/mAs at 1m)	HVL (mm Al)	kV T/F	Output (mGy/mAs at 1m)	HVL (mm Al)
2W/Rh5	10.9	0.49	25 W/Ag	12.7	0.49
28 W/Rh	12.2	0.50	28 W/Ag	14.7	0.51
31 W/Rh	13.6	0.51	31 W/Ag	16.6	0.53
34 W/Rh	15.0	0.52	34 W/Ag	18.5	0.54
37 W/Rh	16.4	0.53	37 W/Ag	20.4	0.56

3.2 Detector response

The detector was found to have a linear response, with an offset of 50, as shown in Figure 5.

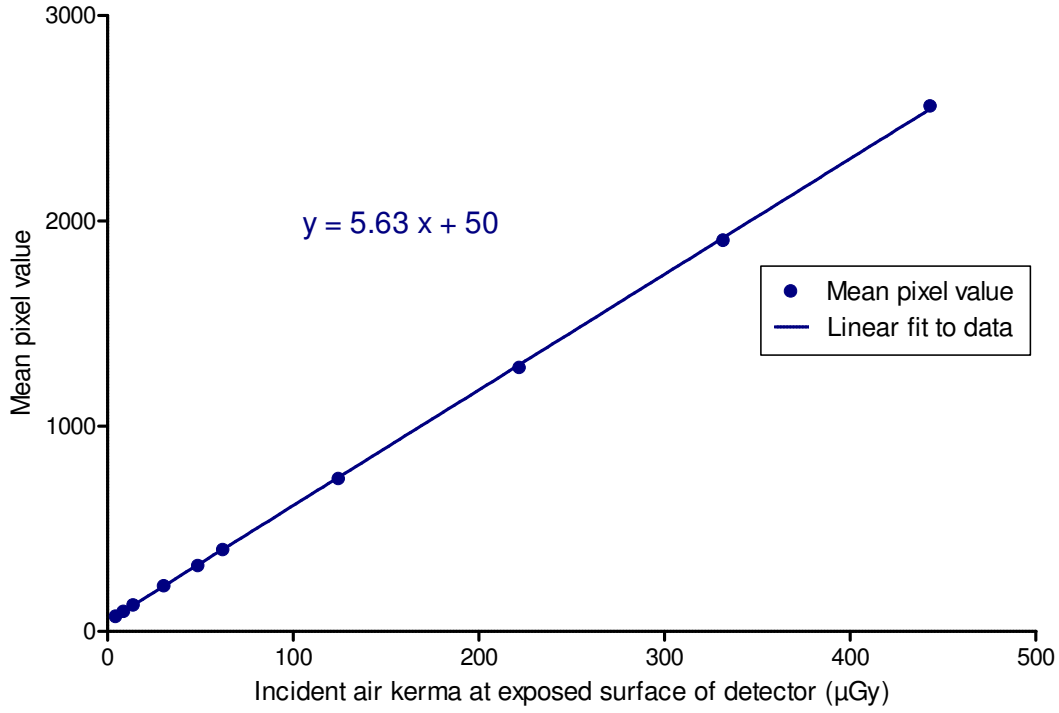

Figure 5 Detector response.

3.3 AEC performance

3.3.1 Dose

The mean glandular doses for breasts simulated with PMMA exposed under AEC control are shown in Table 5 and Figure 6. At all thicknesses the dose was below the remedial level in the NHSBSP protocol (which is the same as the maximum acceptable level in the European protocol). The pre-exposure pulse used in AEC modes is 5 mAs for compressed breast thicknesses less than 50 mm, and 10 mAs for thicknesses equal to or greater than 50 mm. This contributes to the mean glandular dose but is not used to produce the digital image.

Table 5 Mean glandular dose for simulated breasts (Autofilter mode)

PMMA thickness (mm)	Equivalent breast thickness (mm)	kV	Target	Filter	mAs*	MGD (mGy)	NHSBSP remedial level (mGy)
20	21	25	W	Rh	50.6	0.61	> 1.0
30	32	26	W	Rh	76	0.83	> 1.5
40	45	28	W	Rh	100	1.15	> 2.0
45	53	29	W	Rh	117	1.54	> 2.5
50	60	31	W	Rh	115	1.71	> 3.0
60	75	31	W	Ag	116	2.25	> 4.5
70	90	34	W	Ag	112	2.42	> 6.5

*mAs values here include pre-exposure mAs, as this contributes to the MGD.

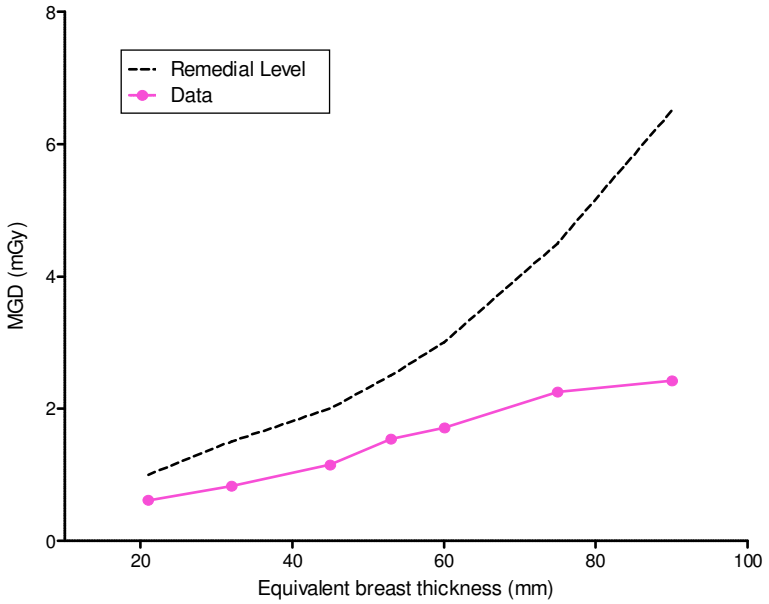

Figure 6 MGD for different thicknesses of simulated breasts using the Autofilter mode.

3.3.2 CNR

The results of the contrast and CNR measurements are shown in Table 5 and Figure 7. The CNR required to meet the minimum acceptable and achievable image quality standards at the 60 mm breast thickness have been calculated and are shown in Table 6 and Figure 7. The CNR required at each thickness to meet the limiting values for CNR in the European protocol are also shown.

Table 6 Contrast and CNR measurements using AEC

Equivalent breast thickness (mm)	kV target/ filter	mAs*	Background pixel value	% contrast for 0.2 mm Al	Measured CNR	CNR at minimum acceptable IQ	CNR at achievable IQ	CNR to meet European limiting value	European limiting values for relative CNR
21	25 W Rh	46	626	17.3%	11.25	4.18	6.09	4.81	>115
32	26 W Rh	71	624	15.9%	10.16	4.18	6.09	4.60	>110
45	28 W Rh	95	623	14.7%	9.15	4.18	6.09	4.39	>105
53	29 W Rh	107	617	14.0%	8.59	4.18	6.09	4.31	>103
60	31 W Rh	105	619	12.6%	7.55	4.18	6.09	4.18	>100
75	31 W Ag	106	712	10.7%	6.70	4.18	6.09	3.97	>95
90	34 W Ag	102	708	9.0%	5.38	4.18	6.09	3.76	>90

*mAs values here do not include pre-exposure mAs, as this does not contribute to the image.

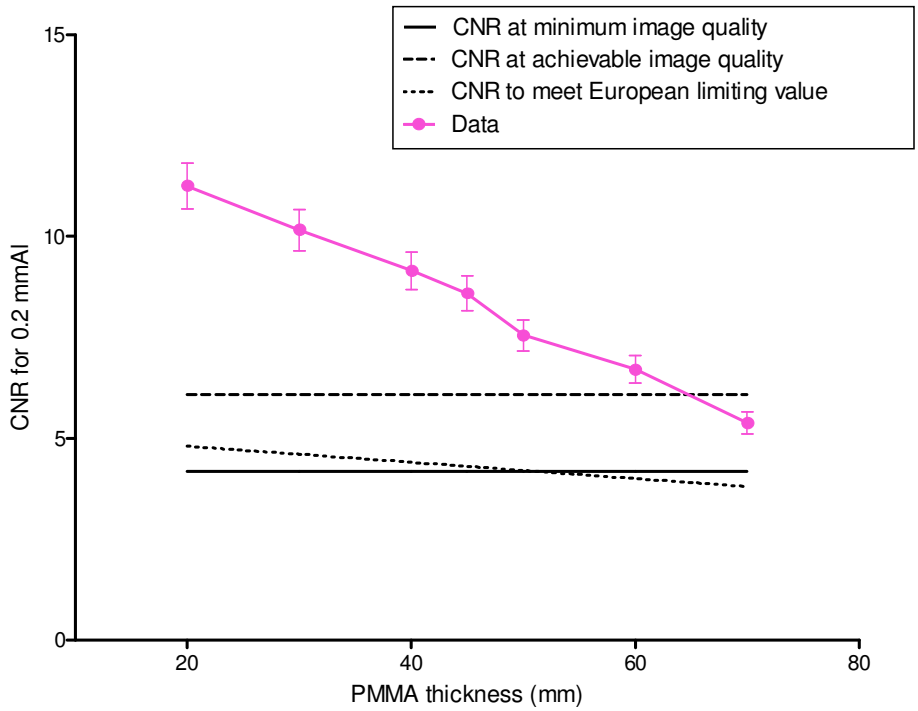

Figure 7 Measured CNR compared with the limiting values in the European protocol for the system. (Error bars indicate 95% confidence limits.)

3.3.3 AEC performance for local dense areas

It is expected that when the AEC adjusts for locally dense areas the SNR will remain constant with increasing thickness of extra PMMA. The results presented in Table 7 and Figure 8 show that the SNR first decreases with thickness and then returns to a constant value close to that with no added attenuation.

Table 7 AEC performance for local dense areas (Autofilter mode)

Attenuation (mm PMMA)	Target/ filter	Tube voltage (kV)	Tube load (mAs)	SNR
30	W/Rh	28	50	57.8
32	W/Rh	28	54	57.2
34	W/Rh	28	61	54.4
36	W/Rh	28	65	50.9
38	W/Rh	28	68	48.6
40	W/Rh	28	67	48.1
42	W/Rh	28	88	51.6
44	W/Rh	28	126	60.2
46	W/Rh	28	139	58.9
48	W/Rh	28	153	58.9

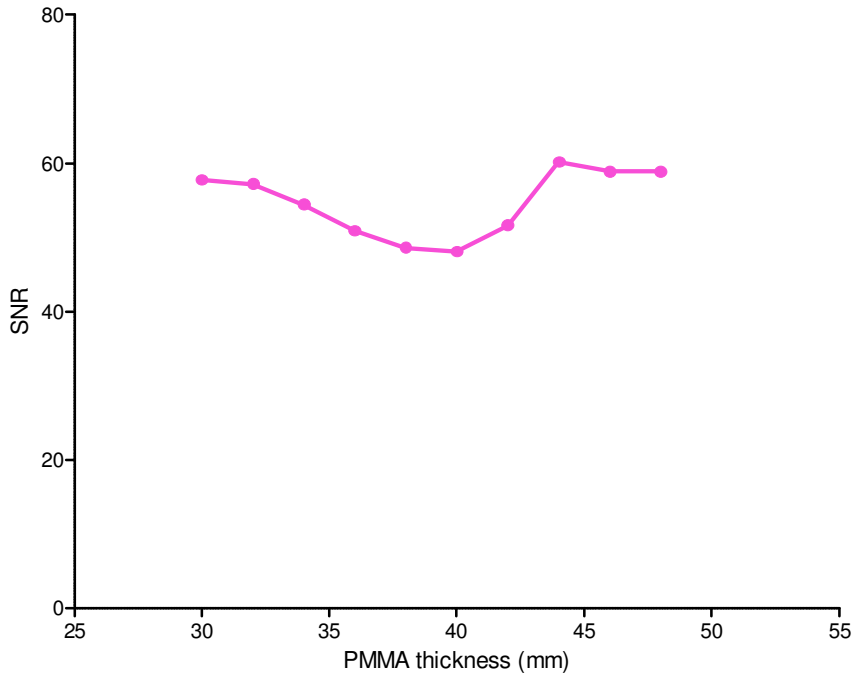

Figure 8 AEC performance for local dense areas.

3.4 Noise measurements

The variation in noise with dose was analysed by plotting the standard deviation in pixel values against the detector entrance air kerma as shown in Figure 9. The fitted power curve has an index of 0.504. If quantum noise sources alone were present the data would form a straight line with an index of 0.5. The data deviates from a straight line at lower doses owing to the presence of electronic noise. This is normal for such systems and quantum noise was the dominant noise source.

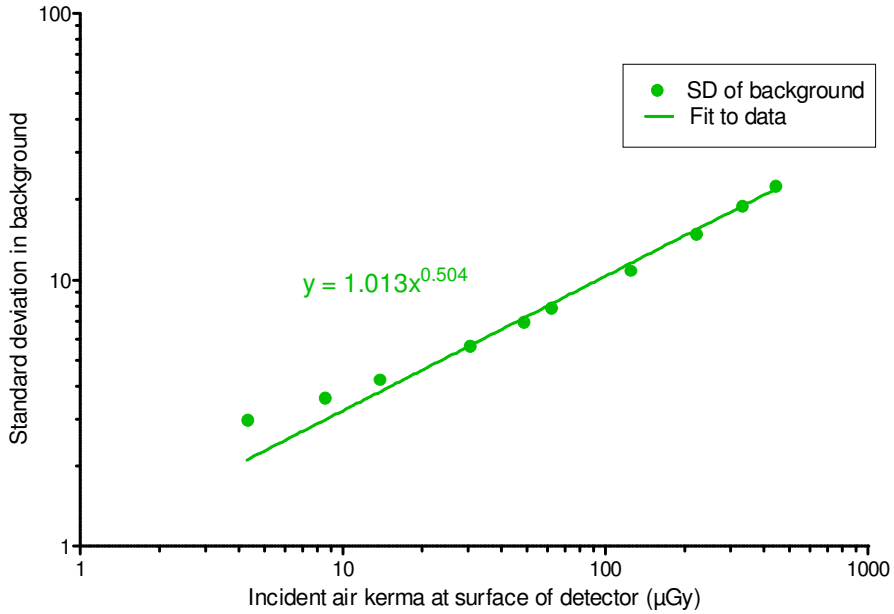

Figure 9 Standard deviation of pixel values versus air kerma at detector.

Figure 10 is an alternative way of presenting the data and shows the relative noise at different entrance air kerma. The estimated relative contributions of electronic, structural and quantum noise are shown and the quadratic sum of these contributions fitted to the measured noise (using equation 3). Figure 11 shows the different amounts of variance caused by each component. Quantum noise predominates over the clinical range.

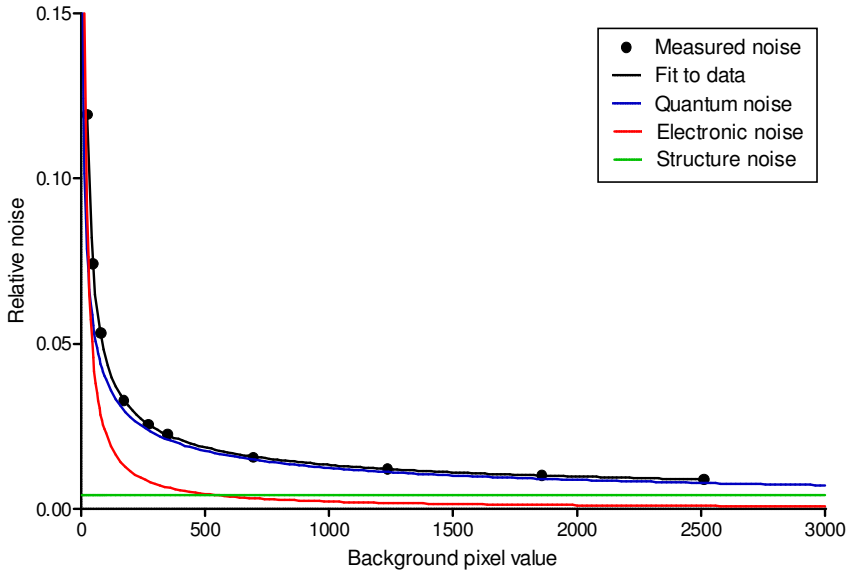

Figure 10 Relative noise and noise components at different pixel values.

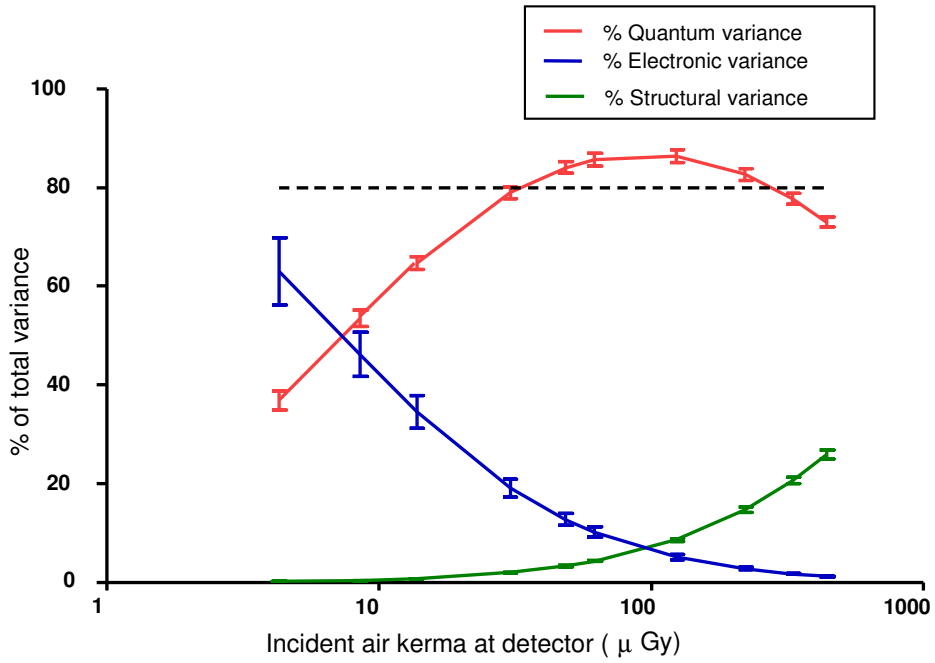

Figure 11 Each noise component as a percentage of the total variance. The percentage quantum variance is compared with a limit of 80%. The errors were estimated assuming that the errors in each of the components were independent.

3.5 Image quality measurements

The first exposures of the image quality phantom were made using the AEC in standard mode to select the beam quality and exposure factors. This resulted in the selection of 31 kV W/Rh and 115 mAs and an MGD of 1.55 mGy to an equivalent breast (60 mm thick). Subsequent image quality measurements were made by manual selection, at a range of mAs values between approximately one quarter and double the AEC-selected mAs, and at the same beam quality as shown in Table 8.

Table 8 Images acquired for image quality measurement

Exposure mode	kV target/filter	Tube loading (mAs)	Mean glandular dose to equivalent breasts 60mm thick (mGy)	Number of CDMAM images acquired and analysed
manual	31 kV W/Rh	30	0.41	16
manual	31 kV W/Rh	60	0.81	16
manual	31 kV W/Rh	90	1.22	16
manual	31 kV W/Rh	120	1.62	16
manual	31 kV W/Rh	180	2.43	16
manual	31 kV W/Rh	240	3.24	16

The contrast detail curves at the different dose levels are shown in Figure 12a and 12b for human and automatic reading of the images. The threshold gold thicknesses for different diameters and the different dose levels for the two systems are shown in Table 9, along with the minimum and achievable threshold values from the NHSBSP protocol (which are the same as the European protocol). The data in Table 9 are taken from the fitted curves rather than the raw data.

The measured threshold gold thicknesses are plotted against the MGD for an equivalent breast for the 0.1 and 0.25 mm detail sizes in Figure 13. The curves in Figure 13 were interpolated to find the doses required to meet the minimum acceptable and achievable threshold gold thicknesses in Table 9. A similar procedure was used to determine the doses required to meet the minimum acceptable and achievable image quality levels for detail sizes from 0.1 to 1.0 mm, as shown in Figure 14.

Table 9a Average threshold gold thicknesses for different detail diameters for three doses using 31 kV W/Rh and automatically predicted data

Dia-meter (mm)	Threshold gold thickness (µm)							
	Accept-able value	Achiev-able value	MGD = 0.41mGy	MGD = 0.81 mGy	MGD = 1.22 mGy	MGD = 1.62 mGy	MGD = 2.43 mGy	MGD = 3.24 mGy
0.1	1.680	1.100	1.986 ± 0.190	1.155 ± 0.111	0.885 ± 0.085	0.818 ± 0.078	0.597 ± 0.057	0.477 ± 0.046
0.25	0.352	0.244	0.329 ± 0.023	0.264 ± 0.019	0.199 ± 0.014	0.174 ± 0.012	0.155 ± 0.011	0.156 ± 0.011
0.5	0.150	0.103	0.145 ± 0.010	0.111 ± 0.007	0.100 ± 0.007	0.093 ± 0.006	0.075 ± 0.005	0.070 ± 0.005
1	0.091	0.056	0.094 ± 0.007	0.063 ± 0.005	0.054 ± 0.004	0.045 ± 0.003	0.037 ± 0.003	0.032 ± 0.002

Table 9b Average threshold gold thicknesses for different detail diameters for three doses using 31 kV W/Rh and human data

Dia-meter (mm)	Threshold gold thickness (µm)							
	Accept-able value	Achiev-able value	MGD = 0.41mGy	MGD = 0.81 mGy	MGD = 1.22 mGy	MGD = 1.62 mGy	MGD = 2.43 mGy	MGD = 3.24 mGy
0.1	1.680	1.100	2.195 ± 0.22	1.311 ± 0.131	0.978 ± 0.098	0.984 ± 0.098	0.751 ± 0.075	0.778 ± 0.078
0.25	0.352	0.244	0.512 ± 0.051	0.279 ± 0.028	0.226 ± 0.023	0.195 ± 0.02	0.168 ± 0.017	0.153 ± 0.015
0.5	0.150	0.103	0.117 ± 0.012	0.128 ± 0.013	0.106 ± 0.011	0.092 ± 0.009	0.079 ± 0.008	0.068 ± 0.007
1	0.091	0.056	0.078 ± 0.008	0.059 ± 0.006	0.053 ± 0.005	0.046 ± 0.005	0.044 ± 0.004	0.038 ± 0.004

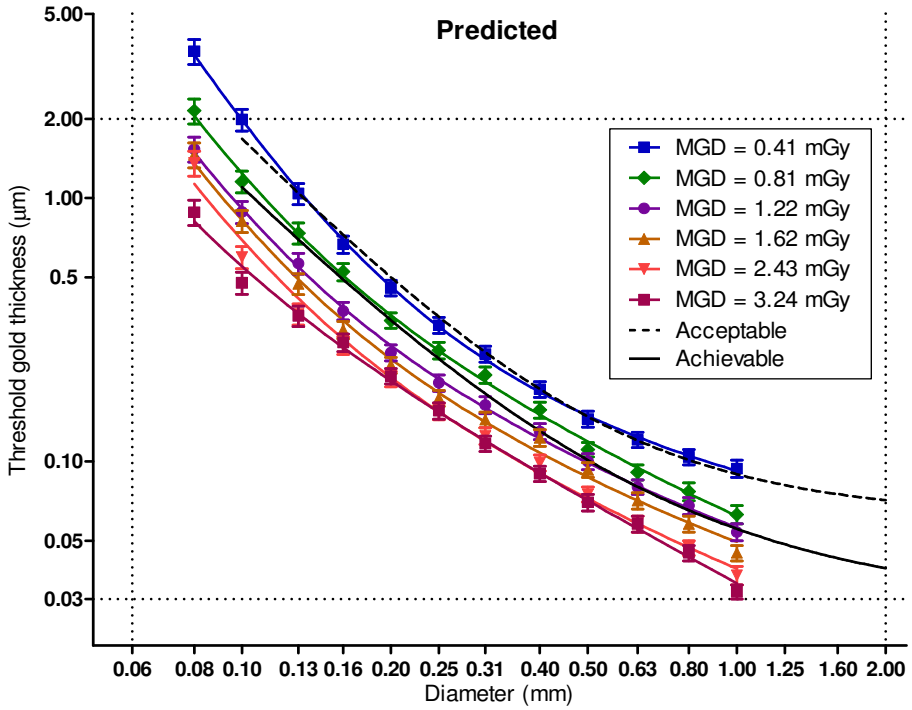

Figure 12a Contrast-detail curves for six doses at 31 kV W/Rh using predicted results from automated reading. The 1.62 mGy dose corresponds to the AEC selection. (Error bars indicate 95% confidence limits.)

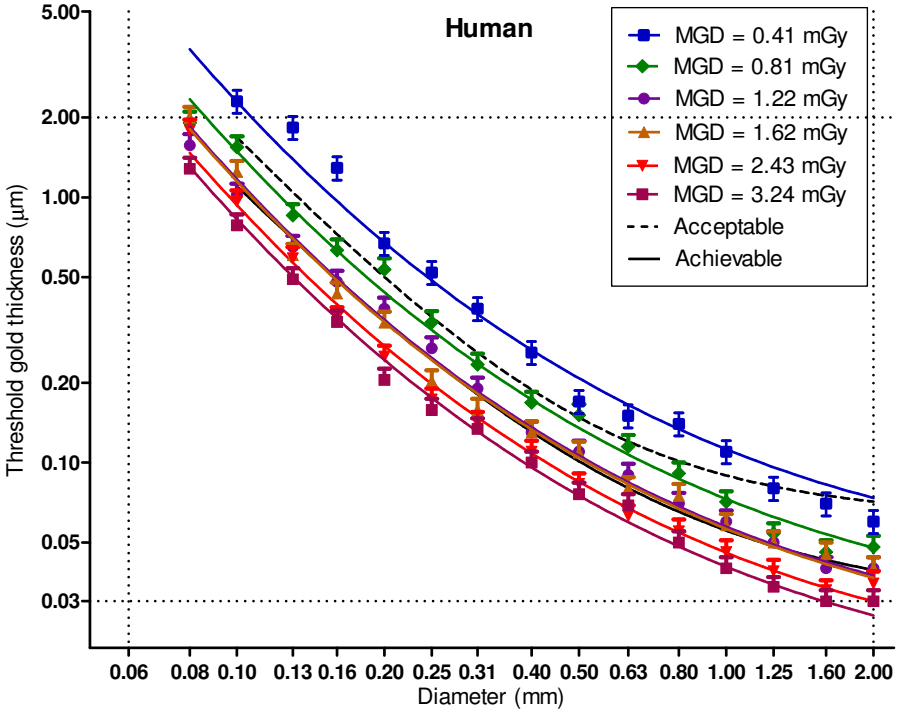

Figure 12b Contrast-detail curves for the five doses at 31 kV W/Rh from human reading. The 1.62 mGy dose corresponds to the AEC selection. Error bars indicate 95% confidence limits.

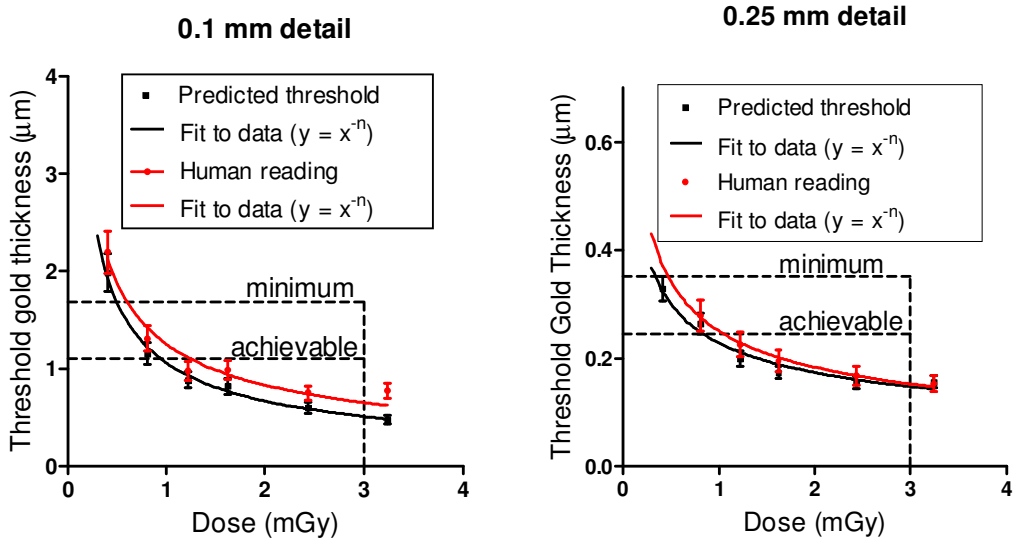

Figure 13 Threshold gold thickness at different doses. (Error bars indicate 95% confidence limits.) The doses are for a breast equivalent to a 5 cm thickness of PMMA.

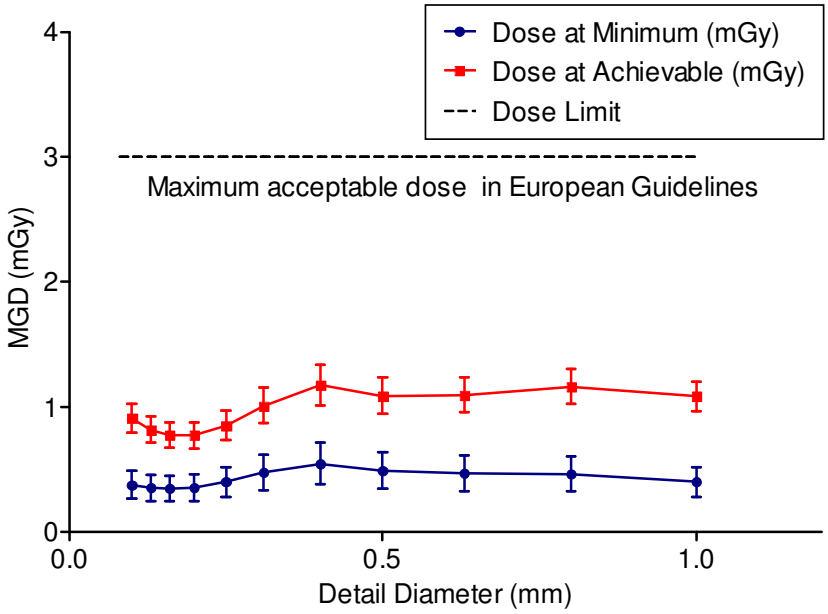

Figure 14 .The MGD calculated to be necessary to reach the achievable and minimum acceptable image quality levels at different detail sizes using 31 kV W/Rh for an equivalent breast 60 mm thick. Based on predicted threshold gold thicknesses. (Error bars indicate 95% confidence limits.)

3.6 Comparison with other systems

The MGDs to reach the minimum and achievable image quality standards in the NHSBSP protocol have been estimated from the curves shown in Figure 13. (The error in estimating these doses depends on the accuracy of the curve fitting procedure and pooled data for several systems has been used to estimate the 95% confidence limits of around 20%.) These doses are shown against similar data for other models of digital mammography system in Tables 10 and 11 and Figures 15 to 18. The data for the other systems has been determined in the same way as described in this report and the results published previously.[3, 8-19] The data for film–screens represent an average value which was determined using a variety of modern film–screen systems.

Table 10 The MGD for different systems to reach the minimum threshold gold thickness for 0.1 and 0.25 mm details.

System	MGD (mGy) for 0.1 mm		MGD (mGy) for 0.25 mm	
	Human	Predicted	Human	Predicted
Sectra MDM-L30	0.41		0.41	0.42
Siemens Novation*	0.54	0.59	0.47	0.67
Siemens Inspiration	0.97	0.76	0.87	0.60
Fuji Amulet	0.62	0.67	0.74	0.71
Hologic Dimensions	0.56	0.38	0.65	0.40
Hologic Selenia (Mo)	0.85	0.55	0.80	0.53
Hologic Selenia (W)	0.58	0.71	0.65	0.64
GE Essential	0.60	0.49	0.50	0.49
GE DS	1.01	0.82	0.87	0.83
IMS Giotto (W)	1.07	1.38	0.91	1.17
Film-screen	1.17	1.30	1.07	1.36
Agfa CR85-X (NIP)	1.24	1.27	1.06	0.96
Agfa CR (MM3.0)†	2.54	2.32	1.45	1.54
Fuji Profect CR	1.67	1.78	1.45	1.35
Carestream CR (EHR-M2)	2.29	2.34	1.45	1.80
Konica Minolta (CP-1M)	1.60	1.47	1.12	0.99

*Data are the mean of measurements for two systems in NHSBSP Equipment Report 0710.[12]
†Data are the mean of measurements shown in NHSBSP Equipment Reports 0707[11] and 0905.[18]

Table 11 The MGD for different systems to reach the achievable threshold gold thickness for 0.1 and 0.25 mm details.

	MGD (mGy) for 0.1 mm		MGD (mGy) for 0.25 mm	
	Human	Predicted	Human	Predicted
Sectra MDM	1.27	1.74	1.37	0.95
Siemens Novation‡	1.30	1.26	1.00	1.37
Siemens Inspiration	2.06	1.27	1.68	1.16
Fuji Amulet	1.40	1.13	1.50	1.41
Hologic Dimensions	1.29	0.91	1.23	0.85
Hologic Selenia (Mo)	1.84	1.19	1.68	1.12
Hologic Selenia (W)	1.66	1.37	1.61	1.48
GE Essential	1.57	1.13	1.14	1.03
GE DS	2.35	1.57	1.80	1.87
IMS Giotto (W)	2.33	2.73	1.77	2.11
Film-screen	2.48	3.03	2.19	2.83
Agfa CR (NIP)	3.22	2.47	2.40	2.34
Agfa CR (MM3.0)§	5.21	5.14	3.72	3.82
Fuji Profect CR	4.26	3.29	3.52	2.65
Carestream CR (EHR-M2)	5.34	5.45	3.03	3.74
Konica Minolta CR (CP-1M)	4.53	3.45	2.73	2.08

‡ Data are the mean of measurements for two systems in NHSBSP Equipment Report 0710.[12]
§ Data are the mean of measurements shown in NHSBSP Equipment Reports 0707[11] and 0905.[18]

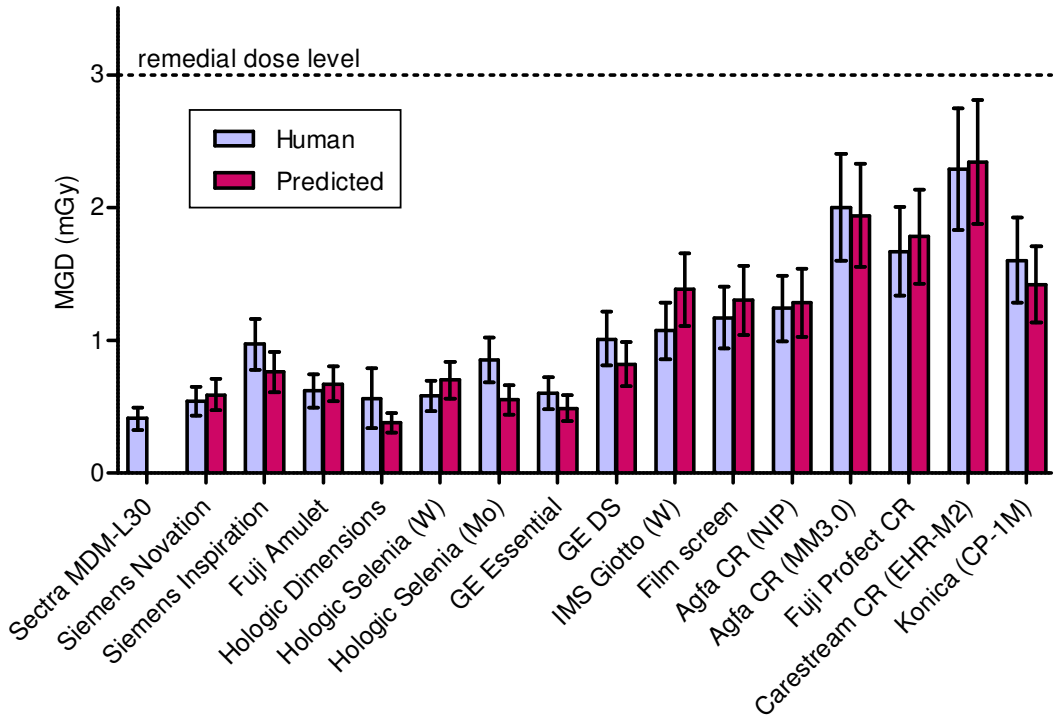

Figure 15 Dose to reach minimum acceptable image quality standard for 0.1 mm detail. (Error bars indicate 95% confidence limits.)

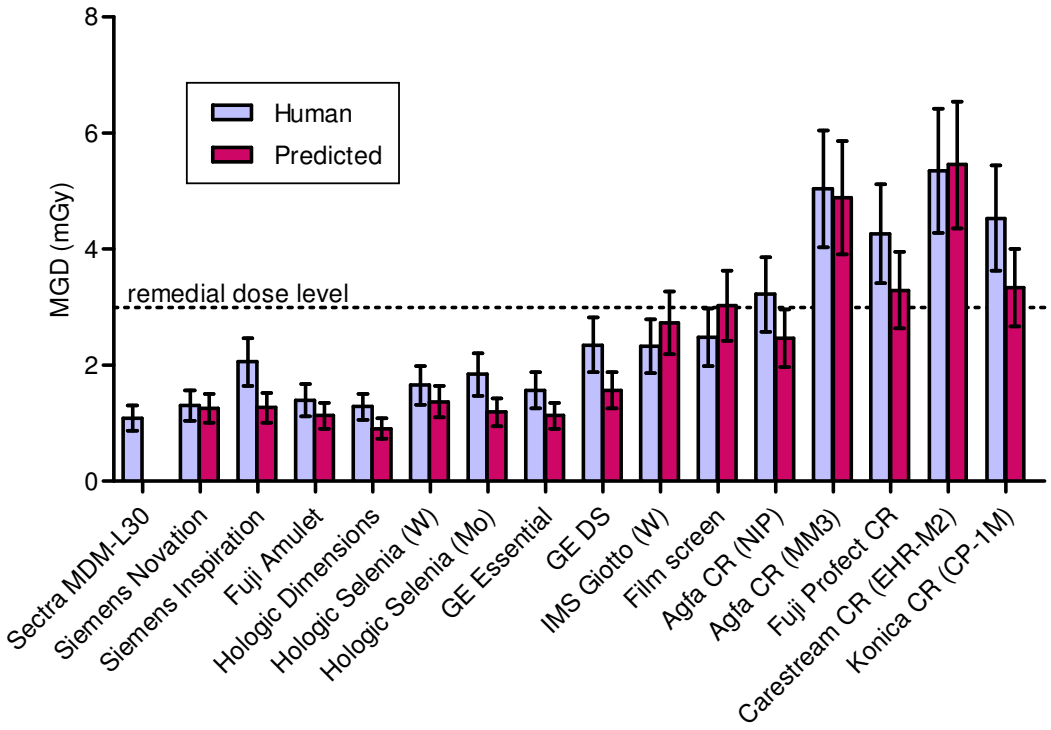

Figure 16 Dose to reach achievable image quality standard for 0.1 mm detail. (Error bars indicate 95% confidence limits.)

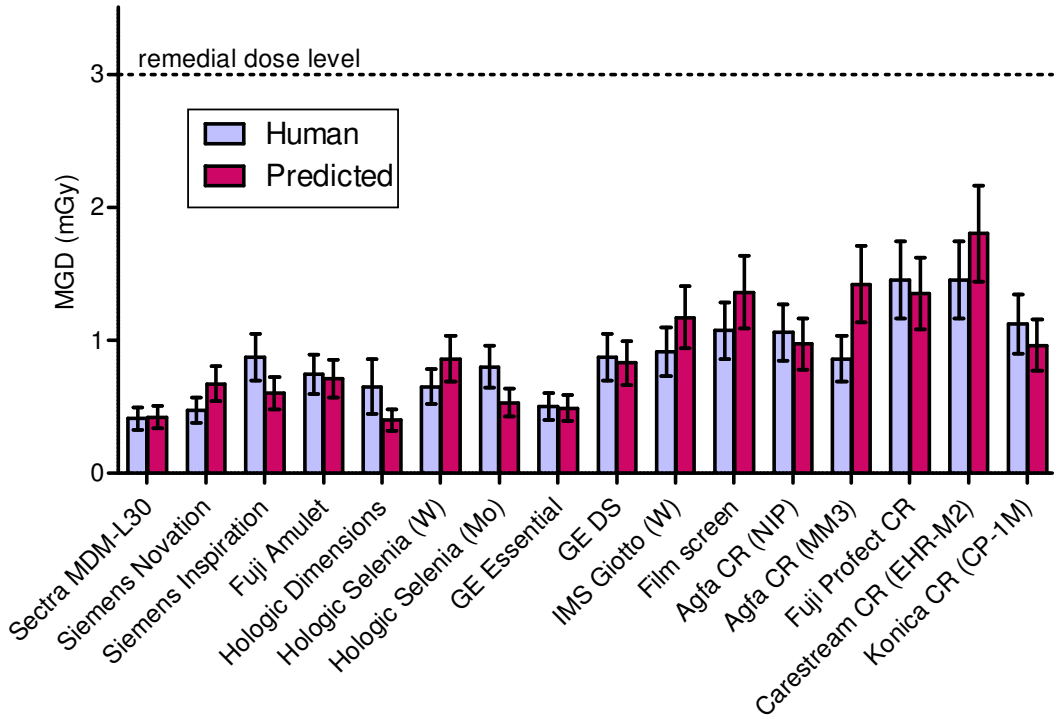

Figure 17 Dose to reach minimum acceptable image quality standard for 0.25 mm detail. (Error bars indicate 95% confidence limits.)

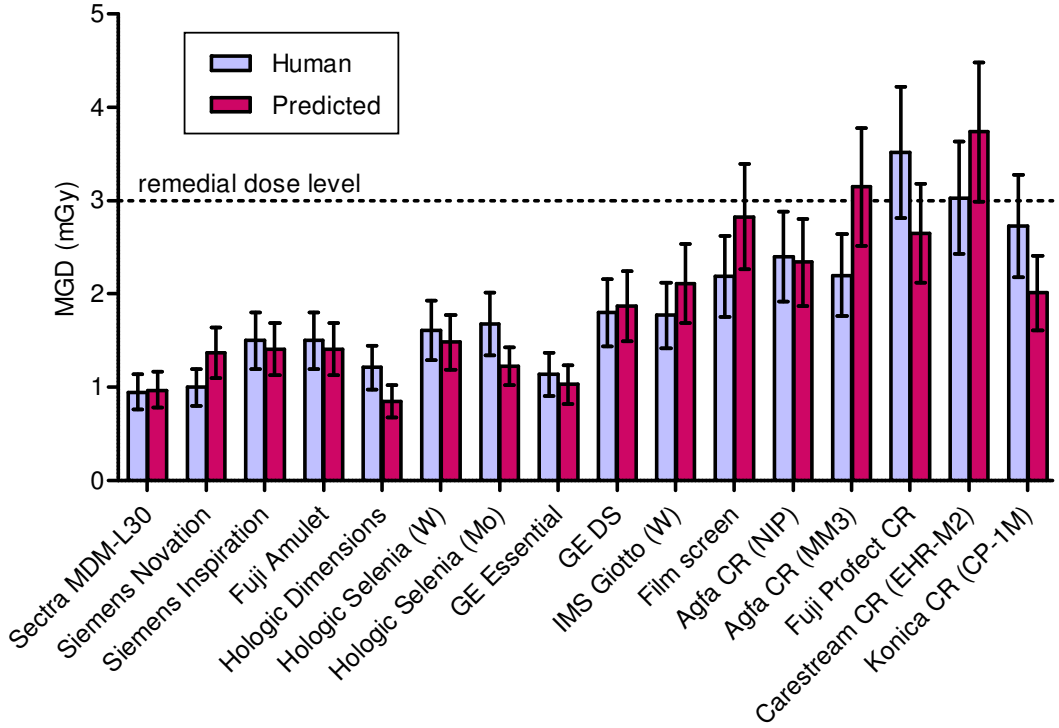

Figure 18 Dose to reach achievable image quality standard for 0.25 mm detail. (Error bars indicate 95% confidence limits.)

3.7 Image retention

The results are shown in Table 12.

Table 12 Image retention factor

ROI	pixel value
1	671.5
2	672.3
3	724.8
Image retention factor: 0.016	

3.8 Detector performance

The MTF is shown in Figure 19 for the two orthogonal directions. Figure 20 shows the DQE averaged in the two orthogonal directions for a range of entrance surface air kerma (ESAK). The MTF and DQE measurements were interpolated to show values at standard frequencies in Table 13.

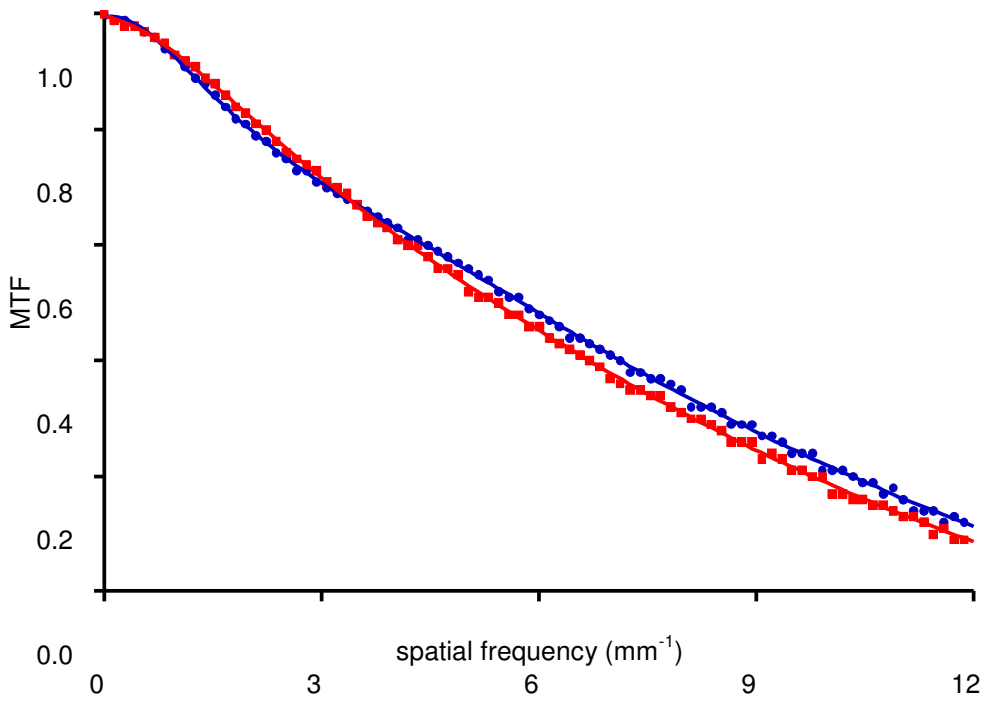

Figure 19 Pre-sampling MTF.

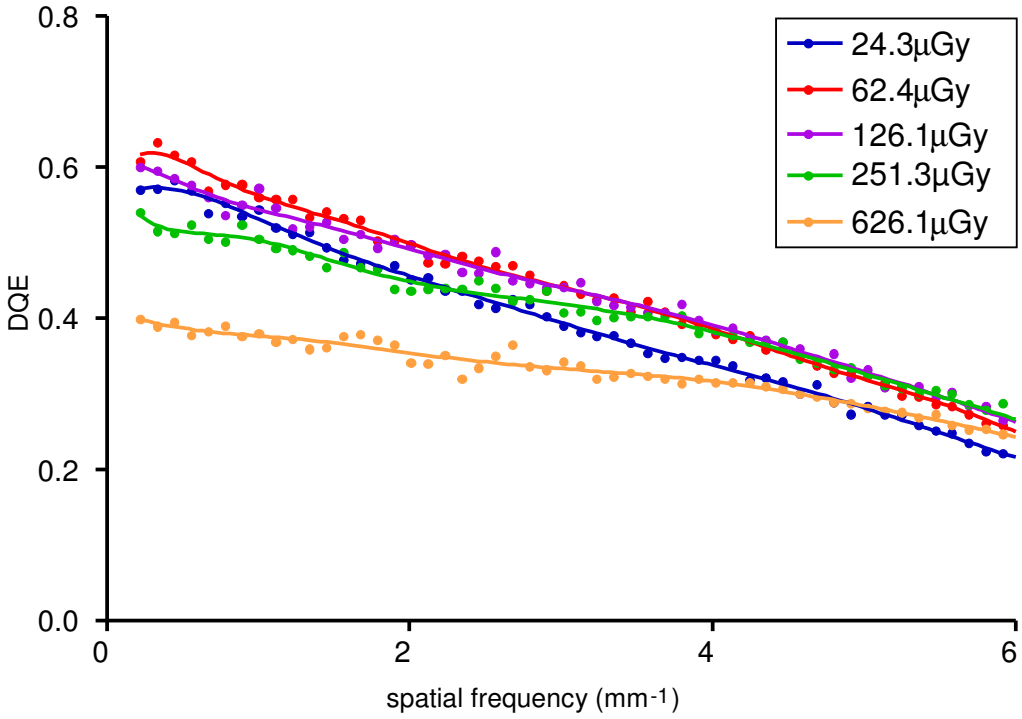

Figure 20 DQE averaged in both directions using 28kV W/Rh and a range of entrance air kerma.

Table 13 MTF and DQE measurements at standard frequencies (DQE at 126.1 uGy).

Frequency (mm^{-1})	MTF (u)	MTF (v)	MTF (uv)	DQE (uv)
0.0	0.99	1.00	0.99	0.61
0.5	0.98	0.97	0.97	0.58
1.0	0.92	0.93	0.93	0.54
1.5	0.86	0.88	0.87	0.52
2.0	0.80	0.82	0.81	0.49
2.5	0.75	0.77	0.76	0.46
3.0	0.71	0.72	0.71	0.44
3.5	0.67	0.67	0.67	0.42
4.0	0.63	0.62	0.63	0.39
4.5	0.60	0.58	0.58	0.36
5.0	0.56	0.53	0.55	0.33
5.5	0.52	0.49	0.51	0.30
6.0	0.48	0.45	0.47	0.26
6.5	0.45	0.41	0.43	0.23
7.0	0.41	0.38	0.39	0.19
7.5	0.37	0.34	0.36	0.014

3.9 Optimisation

The target CNR corresponding to the achievable image quality was calculated to be 6.09. The MGD required to reach this target CNR for each beam quality and different thicknesses of PMMA is shown in Figure 21. From these data the optimal beam qualities were selected and are shown in Table 14.

Table 14 Optimal factors to produce achievable image quality (where CNR = 6.09)

PMMA thickness	kV target/ filter	Background pixel value	mAs	MGD (mGy)	MGD (mGy) when AEC selected factors used	% change in dose if optimal factors used (cf AEC selection)	Remedial dose level in NHSBSP protocol (mGy)
20	25 W/Rh	221	17	0.21	0.61	-66%	1.0
30	25 W/Rh	245	38	0.35	0.83	-58%	1.5
40	25 W/Rh	264	75	0.58	1.15	-50%	2.0
45	28 W/Ag	422	53	0.82	1.54	-47%	2.5
50	28 W/Ag	434	71	1.02	1.71	-40%	3.0
60	28 W/Ag	487	132	1.77	2.25	-21%	4.5
70	28 W/Ag	506	229	2.71	2.42	12%	6.5

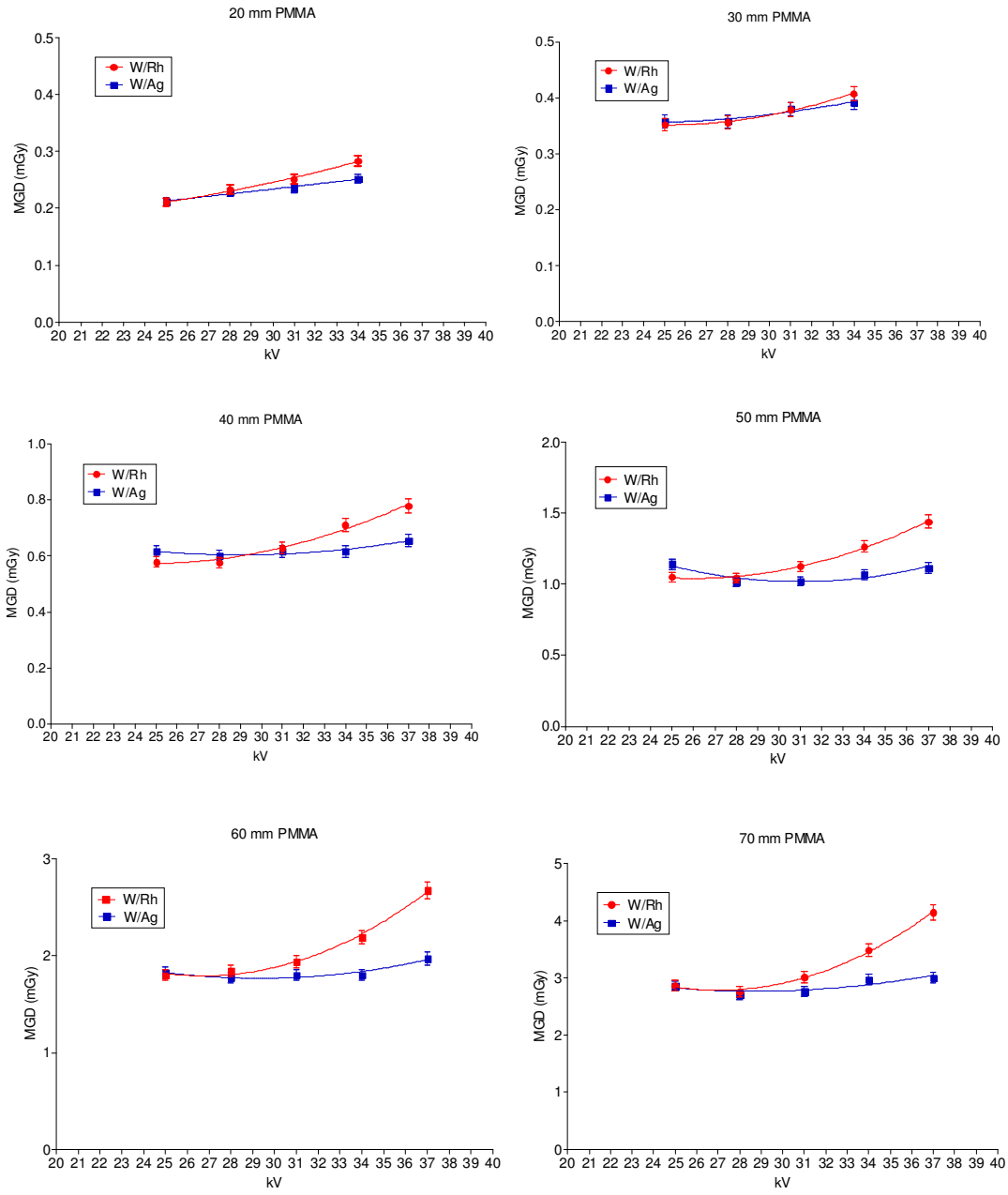

Figure 21 MGD to reach the achievable image quality standard in the NHSBSP protocol. (Error bars indicate 95% confidence limits.)

4. DISCUSSION

As expected, the detector response was linear with an offset of about 50 (pixel value). The noise analysis confirmed that quantum noise is the dominant noise source. As with most systems there was also evidence of some electronic and structural noise. The AEC resulted in doses to simulated breasts that were well below the limits in the NHSBSP protocol. The dose for the standard breast simulated with 45 mm of PMMA was 1.54 mGy. At this thickness an upper limit of 2.5 mGy is applied by the NHSBSP.

The AEC settings resulted in background pixel values of about 620 for the W/Rh target/filter combination and about 710 for W/Ag, corresponding to incident air kerma of approximately 100 µGy. The net result of these choices was that the CNR values were relatively high for thinner breasts but dropped with increasing breast thickness. However the target CNR for achievable image quality was exceeded at all thicknesses except 7cm PMMA (Figure 7).

The AEC test for dense areas showed a decrease followed by an increase in SNR as the thickness of extra attenuation increased. The AEC's choice of exposure is stated by the manufacturer to be governed by the pixel values measured in two ROIs, one the minimum and one the average for the whole field of view. The position of the 'average' ROI therefore gradually shifts from entirely outside the extra attenuation to partially and then wholly inside it. The simple geometry of the test dense area does not give a very realistic model of the varying densities which would be present in a clinical image.

The image quality measurements indicated that for the standard thickness tested (equivalent to 50 mm thickness of PMMA: ie 60 mm of typical breast) the image quality for the Hologic Dimensions exceeded the achievable level using the dose selected by the AEC (1.62 mGy using 31 kV W/Rh). A dose of 0.91 ± 0.18 mGy was calculated to be necessary to reach the achievable image quality level using automatic reading. A slightly higher dose of 1.29 ± 0.26 mGy was found to be necessary using human readers. These are relatively low doses compared with the other commercial systems shown in Table 9. The current AEC is designed to provide higher doses which achieve better image quality rather than lowest dose and this seems reasonable given the current state of knowledge. Nonetheless the dose levels are well within current guidelines and compare well with most film–screen systems.

The image retention factor, 0.016, is well below the remedial level of 0.3.

The DQE is greatest for the middle range of entrance air kerma, away from the extremes where electronic and structural noise become significant.

The results of the optimisation study suggest that 25 W/Rh would be optimum for smaller breasts and 28 W/Ag for larger breasts. However the manufacturers' choice of kV, target and filter are essentially optimal and the dose level mostly sufficient to exceed the achievable image quality limits.

5. CONCLUSIONS

The Dimensions system in 2-D mode is capable of producing good image quality for a relatively low radiation dose. The system met the main standards in the NHSBSP and European protocols.

REFERENCES

1. Workman A, Castellano I, Kulama E et al. *Commissioning and Routine Testing of Full Field Digital Mammography Systems*, 2nd edition. NHS Cancer Screening Programmes, 2006 (NHSBSP Equipment Report 0604).
2. Young KC, Johnson B, Bosmans H, Van Engen R. Development of minimum standards for image quality and dose in digital mammography In: *Digital Mammography, Proceedings of the 7th International Workshop on Digital Mammography*, Durham NC, USA, June 2004. (2005).
3. Van Engen R, Young KC, Bosmans H, Thijssen M. The European protocol for the quality control of the physical and technical aspects of mammography screening. In: *European Guidelines for Quality Assurance in Breast Cancer Screening and Diagnosis*, 4th edn. Luxembourg: European Commission, 2006, 732–739.
4. Alsager A, Young KC, Oduko JM. Impact of heel effect and ROI size on the determination of contrast-to-noise ratio for digital mammography systems. In: Hsieh J, Samei eds. *Proceedings of SPIE Medical Imaging*, SPIE Publications, Bellingham WA, 2008, 69134I: 1-11.
5. Young KC, Cook JJH, Oduko JM. Automated and human determination of threshold contrast for digital mammography systems. In: Astley SM, Bradey M, Rose C, Zwiggelaar R, eds. *Proceedings of the 8th International Workshop on Digital Mammography. Lecture Notes in Computer Science*, 2006, 4046:266-272.
6. Young KC, Alsager A, Oduko JM et al. Evaluation of software for reading images of the CDMAM test object to assess digital mammography systems. In: Hsieh J, Samei eds. *Proceedings of SPIE Medical Imaging*, SPIE Publications, Bellingham WA 2008, 69131C: 1-11.
7. IEC 62220-1-2, *Determination of the detective quantum efficiency. Detectors used in mammography. International.* International Electrotechnical Commission (2007).
8. Young KC, Oduko JM. *Evaluation of Kodak DirectView Mammography Computerised Radiography.* NHS Cancer Screening Programmes, 2005 (NHSBSP Equipment Report 0504).
9. Young KC, Oduko JM, Woolley L. *Technical Evaluation of the Hologic Selenia Full Field Digital Mammography System.* NHS Cancer Screening Programmes, 2007 (NHSBSP Equipment Report 0701).
10. Young KC, Oduko JM. *Technical Evaluation of Kodak DirectView Mammography Computerised Radiography System Using EHR-M2 Plates.* NHS Cancer Screening Programmes, 2007 (NHSBSP Equipment Report 0706).
11. Young KC, Oduko JM. *Technical Evaluation of the Agfa CR85-X Mammography System*. NHS Cancer Screening Programmes, 2007 (NHSBSP Equipment Report 0707).
12. Young KC, Oduko JM. *Technical Evaluation of the Siemens Novation Full Field Digital Mammography System*. NHS Cancer Screening Programmes, 2007 (NHSBSP Equipment Report 0710).

13. Young KC, Oduko JM. *Technical Evaluation of the Hologic Selenia Full Field Digital Mammography System with a Tungsten Tube.* NHS Cancer Screening Programmes, 2008 (NHSBSP Equipment Report 0801).

14. Young KC, Oduko JM, Gundogdu O, Alsager A. *Technical Evaluation of the GE Essential Full Field Digital Mammography System.* NHS Cancer Screening Programmes, 2008 (NHSBSP Equipment Report 0803).

15. Oduko JM, Young KC, Alsager A, Gundogdu O. *Technical Evaluation of the IMS Giotto Full Field Digital Mammography System with a Tungsten Tube.* NHS Cancer Screening Programmes, 2008 (NHSBSP Equipment Report 0804).

16. Young KC, Oduko JM Gundogdu O, Alsager A. *Technical Evaluation of the Konica Minolta Regius 190 CR Mammography System and Three Types of Image Plate.* NHS Cancer Screening Programmes, 2008 (NHSBSP Equipment Report 0806).

17. Young KC, Oduko JM Gundogdu O, Asad M. *Technical Evaluation of Profile Automatic Exposure Control Software on GE Essential Full Field Digital Mammography System.* NHS Cancer Screening Programmes, 2009 (NHSBSP Equipment Report 0903).

18. Young KC, Oduko JM, Asad M. *Technical Evaluation of Agfa DX-M Mammography CR Reader with HM5.0 Needle-IP.* NHS Cancer Screening Programmes, 2009 (NHSBSP Equipment Report 0905).

19. Young KC, Oduko JM, Asad M. *Technical Evaluation of Fuji Amulet Full Field Digital Mammography System.* NHS Cancer Screening Programmes, 2009 (NHSBSP Equipment Report 0907).

NHS Cancer Screening Programmes
Fulwood House
Old Fulwood Road
Sheffield
S10 3TH